Scale Formation in Reservoir and Production Equipment During Oil Recovery. III. A Kinetic Model for the Precipitation/Dissolution Reactions

Dag Granbakken,[a,*] Torstein Haarberg,[†] Mette Rollheim,[a] Terje Østvold[a,‡] Peter Read[b] and Terje Schmidt[b]

[a]Institute for Inorganic Chemistry, Norwegian Institute of Technology, N-7034 Trondheim and [b]Den norske stats oljeselskap a.s., PO Box 300, Forus, N-4001 Stavanger, Norway

Granbakken, D., Haarberg, T., Rollheim, M., Østvold, T., Read, P. and Schmidt, T., 1991. Scale Formation in Reservoir and Production Equipment During Oil Recovery. III. A Kinetic Model for the Precipitation/Dissolution Reactions. – Acta Chem. Scand. 45: 892–901.

A kinetic model for the precipitation–dissolution reactions of scale-forming minerals is presented. The model is based on experimental data on the kinetics of these reactions. By combining the kinetic model with an equilibrium model developed previously and a hydrodynamic model for the simultaneous transport of oil, water and gas in the area near the well, in the well and in the production tubing, we are able to estimate in which part of the production system scaling will occur.

Our model calculations on a North Sea well where the tubing had to be pulled up gave a scale build-up profile along the 2800 m long tubing from the bottom to the well head which agreed quantitatively with the scale thickness measured on the tubing.

In two previous papers we have discussed scale formation based on chemical equilibrium in multicomponent water solutions.[1,2] Using a simple hydrodynamic model for liquid transport in a model reservoir, we were able to simulate precipitation and dissolution reactions of scale-forming minerals in the reservoir itself. Owing to relatively large pore volumes and moderate mineral precipitation, no damage to the reservoir itself could be observed as expected. When the oil–water mixture approaches the production well, the pore volume available for liquid transport is drastically reduced. The reduction is inversely proportional to r^2, where r is the distance from the well centre. In the well area relatively large pressure changes are also observed. Since these pressure changes influence the solubility of the scale-forming minerals, scaling is expected in this area of the production system. Owing to the small cross-section for liquid flow, well damage may easily occur.

Since the flow rates are low in the reservoir, we find it sufficient to use equilibrium calculations for estimating scale formation. Because of higher flow rates in the production tube and in the area near the well, however, precipitation kinetics must be taken into account in order to obtain reliable scale prediction in this portion of the production system.

When the oil–water mixture enters the tubing, a relatively simple and reliable hydrodynamic model may be used to simulate liquid flow, and gas flow if the total pressure is below the bubble point pressure of the liquids. Combining this model with our model for mineral precipitation, we are able to simulate scale formation in the tubing, assuming chemical equilibrium for CO_2 between the oil and the water phases.

A kinetic model for mineral precipitation

The kinetics of precipitation and dissolution of five minerals, $CaCO_3$, $BaSO_4$, $SrSO_4$, $CaSO_4$ (anhydrite) and $CaSO_4 \cdot 2H_2O$ (gypsum) have been studied experimentally and the rate equations are presented by using rate equations for these reactions. The kinetics of the CO_2–water system is also included.

In general, the rate equation for precipitation of the five minerals may be given by eqn. (1),[3–23] where MeA(s) is the

$$\frac{d[MeA(s)]}{dt} = k_{prec}\, s[([Me^{2+}][A^{2-}])^{1/2} - (K^{\circ}_{sp}/\gamma^2)^{1/2}]^2 \qquad (1)$$

amount of solid mineral precipitated, t is the time, k_{prec} is the rate constant for precipitation, s is the specific crystal surface area per volume of solution, $[Me^{2+}]$ is the concentration of the cation at time t, $[A^{2-}]$ is the concentration of the anion at time t, K°_{sp} is the thermodynamic solubility product and γ is the mean activity coefficient of MeA in

* Present address: Statens forurensningstilsyn, PO Box 8100, Dep. 0032, Oslo 1, Norway.
† Present address: Hydro Aluminium, Ardal Verk, N-5875 Ardalstangen, Norway.
‡ To whom correspondence should be addressed.

solution. The rate of reaction (1) is assumed to be surface-controlled for all five minerals.

In general, the rate equation[8,13,14,16,18,24,25] for dissolution is given by eqn. (2), which is valid for $BaSO_4$, $SrSO_4$ and

$$\frac{d[MeA(s)]}{dt} = -k_{diss}\, s[(K°_{sp}/\gamma^2)^{1/2} - ([Me^{2+}][A^{2-}])^{1/2}]^2 \qquad (2)$$

$CaSO_4$ (anhydrite). The dissolution process is also assumed to be surface-controlled. For $CaSO_4 \cdot 2H_2O$ (gypsum), for which the dissolution reaction is assumed to be diffusion-controlled, the rate equation is first order.

Eqn. (2) is a simplified rate equation for $CaCO_3$ dissolution.[25] In order to take into consideration the effect of pH, which is very important in $CaCO_3$ reactions with water, we have combined eqn. (2) and eqn. (1) for $CaCO_3$ precipitation with an equation which takes into consideration the rate of reactions in the water–CO_2 system. Details are explained below.

All equations, with the exception of gypsum dissolution, are therefore of second order in super- or under-saturation. The equations are based on experimental work in aqueous solutions,[3–25] where, for example, precipitation experiments have been carried out by bringing a supersaturated solution of the mineral into contact with a given amount of crystals of this mineral. Compared to the situation during oil production, where water, oil and gas may be mixed, these experiments are carried out under ideal conditions and may not in a proper way reflect precipitation during oil production. However, we feel that it may be useful to test the results of these laboratory experiment on a real oil production system where scale is formed.

A basic assumption in our model is that the nucleation time is short relative to the time it takes for the precipitating mineral to grow thick layers of scale. This assumption is necessary, since nucleation kinetics are normally different from growth kinetics. Preliminary experimental work on the precipitation of $BaSO_4$ and $SrSO_4$ in steel tubing indicates that this approximation is reasonable.[26]

The rate constants of precipitation and dissolution are functions of temperature.[6,7,15,17,18,22,27] For dissolution the temperature dependence of the rate constants are known for $BaSO_4$,[8,28] $CaSO_4$ (anhydrite)[18] and $CaSO_4$ (gypsum).[24,27] No literature data for the temperature dependence of the rate constants for dissolution of $SrSO_4$ and $CaCO_3$ were found. We have adopted an approximation which may lack accuracy. For $BaSO_4$ some data[13] indicate that the rate constant of dissolution is 35 times the rate constant of precipitation. The same multiplication factor, 35, was also used in our model to relate the rate constants of dissolution to the rate constants of precipitation for $CaCO_3$ and $SrSO_4$.

All the rate constants are given as functions of temperature in Table 1. The influence of pressure and ionic strength on the rate constants are not included in the kinetic model because of a lack of data.

Table 1. Rate constants for precipitation and dissolution of scaling minerals, $k = A \exp(-E_a/RT)$.[a]

Salt	A	E_a/kJ mol	Temperature range/°C	Ref.
Precipitation:				
$CaCO_3$	2.58×10^6	39.2±3.6	15– 35	6[b,c]
$BaSO_4$	3.05×10^4	33.5±4.0	25–125	7[b,c]
$SrSO_4$	2.17×10^8	67	25– 45	15[b,c]
$CaSO_4$ (A)[d]	9.8×10^3	58±9	120–150[b]	17[b]
			130–140[c]	18[c]
$CaSO_4$ (G)[d]	2.39×10^7	63±2	15– 45[b]	22[b]
			70[c]	27[c]
Dissolution:				
$CaCO_3$[e]				13
$BaSO_4$[f]	2.73×10^9	50±30	25– 35[b]	28[b]
			25[c]	8[c]
$SrSO_4$[e]				13
$CaSO_4$ (A)	31.3×10^3	61±10	130–140	18[b,c]
$CaSO_4$ (G)[g]	1.95×10^6	41.8±6.3	10– 30	24[b,c]
				27[h]

[a] A, pre-exponential factor; k, rate constant; E_a, energy of activation; R, gas constant; T, temperature in K. [b] For E_a. [c] For k. [d] The energies of activation are taken from Refs. 17 (anhydrite) and 22 (gypsum). The rate constants are taken from Refs. 18 (anhydrite) and 27 (gypsum). Combination of these data gives the rate constant as a function of temperature. [e] The following approximation[13] is adopted in our model: k(dissolution) = 35 k(precipitation). When seed crystals of different morphology were used, the overall dissolution rate constants ranged from 20 to 70 times those of precipitation.[13] [f] The energy of activation was found in Ref. 28. It varied from 20 to 80 kJ mol^{-1}. The rate constant used was found in Ref. 8 at 25 °C. [g] Specific surface area, SSA (s), of $CaSO_4$ (G) given by Ref. 27 were necessary to obtain the rate constants for dissolution of gypsum on the form given in the table. Rate constant data (ks) were obtained from Ref. 24. The seed crystals used in both investigations[24,27] were obtained by similar methods. [h] For SSA.

In the rate eqns. (1) and (2) the term s (the specific crystal surface area per volume of solution) is a function of the number of active points for crystallization or dissolution.

In the present model s is assumed to be proportional to the specific surface area of the inner tubing wall [eqn. (3)],

$$s_{wall} = f_1 A/V \qquad (3)$$

where f_1 is a proportionality factor, A is the surface area of the tubing for a given tube length and V is the volume of the same tube length.

Eqn. (1) describes the amount of precipitate formed from the precipitating mineral as a function of time. In tubing this may be represented by crystal growth directly on active sites for crystallization on the tubing wall, and by the growth of particles present in the bulk of the solution. The number of active sites for crystallization in the bulk

phase is assumed to be proportional to the number of seed crystals present in the solution. The number of seed crystals will vary along the tubing. This is due to the transport of particles from the bulk phase on to the pipe wall, a varying influence of precipitation and nucleation mechanisms and to the removal of precipitated mineral sitting on the tubing wall by the fluid flow.

In a recent experimental study[26] we found that $f_1 >> 1$ as long as $BaSO_4$ precipitates from a water solution. The data also indicated that the number of active sites for crystallization varied linearly with $1/r$, where r was the tube diameter. This is in agreement with the model equation, eqn. (3).

In prescaled tubings the growth of $BaSO_4$ calculated by our model equations explained ca. 90% of the observed scale. The somewhat larger amount found experimentally is probably due to settling of $BaSO_4$ crystals formed in the liquid phase.

However in the calculations presented later in this paper we have assumed, owing to the lack of data for f in the oil–water system, that the number of active sites for crystal growth on the tubing wall is A/V (or $f_1 = 1$). This is a much smaller value than in the pure water system.[26] Setting $f = 1$ may be a rough approximation, but it may still be reasonable in view of the effect oil may have on the effective area for crystal growth.

The rate-determining reactions of dissolution of carbon dioxide in the CO_2–water system are given by eqns. (4) and (5), where k_1, k_{-1}, k_2 and k_{-2} are rate constants. By com-

$$CO_2(aq) + H_2O \underset{k_{-1}}{\overset{k_1}{\rightleftharpoons}} H_2CO_3(aq) \quad (4)$$

$$CO_2(aq) + OH^- \underset{k_{-2}}{\overset{k_2}{\rightleftharpoons}} HCO_3^- \quad (5)$$

bining these two reactions, the rate equation for the dissolution of CO_2 is given by eqn. (6).

$$\frac{d[CO_2(aq)]}{dt} = k_{-1}[H_2CO_3] - k_1[CO_2(aq)]$$

$$- k_2[OH^-][CO_2(aq)] + k_{-2}[HCO_3^-] \quad (6)$$

In Table 2 the rate constants for carbon dioxide hydration kinetics [eqn. (4)] and acid–base reaction kinetics for the forward reaction [eqn. (5)] are given.[29,30]

Table 2. Rate constants, $k = B \exp(C - D/T)$ for CO_2 hydration [k_1, eqn. (4)] and the acid–base reaction kinetics [k_2, eqn. (5)].

k	Temperature range/°C	B	C	D	Ref.
k_1	1–38.5	1×10^{-3}	34.69	9252	29
k_2	0–40	1	31.36	6658.5	30

The relationship between the forward rate constants, k_1 and k_2, and the equilibrium constants for reactions (4) and (5), respectively, are used to obtain the temperature dependence for k_{-1} and k_{-2}.

In the case of precipitation we have six rate equations [for CO_2, $CaCO_3$, $CaSO_4$ (anhydrite), $CaSO_4 \cdot 2H_2O$ (gypsum), $SrSO_4$ and $BaSO_4$] and 18 equations to determine the equilibrium situation.[2] After elimination and simplification, eight equations and eight unknowns remain. These equations are given in Appendix 1, and the corresponding list of symbols is given in Appendix 2.

The set of equations is simultaneously integrated by numerical calculation for any chosen time period. A predesigned numerical model using backward differentiation formulae of orders one to five is used in solving the set of equations.

A model for the simulation of flow in the production well area and the production tube

In order to simulate precipitation in the production system, it is necessary to have a flow model combined with an equilibrium or kinetic model.

The flow model is based on a principle called the Lagrangian method. This uses a coordinate system that moves at the average velocity of the flowing fluid. The solute concentration changes are determined for packets of fluid that move through the pipeline. A Lagrangian mass element is not spatially fixed in time but is allowed to change its geometric dimensions to accomodate the growth of scale. The mass element consists of water and oil (and gas when the total pressure is below the bubble point pressure). This mass element is moved from the reservoir through the well area to the top of the production tube.

A radial model is used for the production well area. To describe radial flow in a porous medium, the basic differential equation, eqn. (7) is used,[31] in which φ is the poros-

$$\frac{1}{r}\frac{\partial}{\partial r}\left(\frac{k\varrho}{\mu} r \frac{\partial P}{\partial r}\right) = \varkappa\varphi\varrho \frac{\partial P}{\partial t} \quad (7)$$

ity, k is the permeability, μ is the viscosity, $\varkappa$ is the compressibility, P is the pressure, ϱ is the density and r is the distance from the tube centre.

Modifying eqn. (7) to fit flow in a reservoir close to the production well and assuming steady-state flow conditions, gives it the form of eqn. (8), where h is the height of a

$$\frac{\partial P}{\partial r} = \frac{q_o\mu}{2\pi k_o h}\left(\frac{1}{r}\right) \quad (8)$$

model reservoir with constant geophysical properties, k_o is the relative permeability for oil and q_o is the volume flow of oil. We have assumed a constant temperature in the well area.

To simulate the flow in the production tube a commercial simulator called Vertical Flow Performance (VFP)[32] is used. VFP is a multiphase program which calculates the pressure traverse in steps up and down the well bore between the tubing head and the botton hole depth. It can supply detailed information on the pressure traverse in the well for particular sets of flow conditions, by using different multiphase flow correlations.

The temperature in the tubing is calculated using an enthalpy balance. The surroundings are assumed to have a linear temperature gradient.

The Lagrangian mass element is moved from the reservoir to the top of the production tube. For each calculation point either the equilibrium model or the kinetic model calculates the mineral precipitation. In addition to the aqueous composition both models, at the point of calculation, need information on (i) the volume of water, oil and gas, (ii) the pressure, (iii) the temperature and (iv) the oil density in order to calculate mineral precipitation.

The kinetic model also needs the duration of the time-step that the Lagrangian mass element uses from one calculation point to another. In the well area this time is calculated using eqn. (9),where r_1 is the radius of the last calcula-

$$\tau = \pi h(r^2_1 - r^2_2)\varphi/q_w \quad (9)$$

tion point, r_2 is the radius of the new calculation point, h is the layer height, q_w is the volume flow of water and φ (as before) is the porosity.

In the production tube this time is calculated using eqn. (10), where L_w is the distance between last and new calcula-

$$\tau = L_w/\mathrm{HAL} \quad (10)$$

tion point and HAL is the flow velocity of water (from VFP).

Results

Fig. 1 illustrates how the concentration of Ba^{2+} may vary with time in a supersaturated solution of $BaSO_4$ during crystallization. Temperature and pressure have constant values of 25 °C and 1 atm, respectively. The four curves A–D are obtained using eqn. (1) and experimental values of $k \times s$.[14] In these four experiments different types of seed crystals were used. The specific surface areas (SSA) for the four types of seed used in the experiments are given in Table 3. The curves E (tube segment diameter = 0.1 m) and F (tube segment diameter = 0.01 m) are obtained using eqn. (1) with a k-value given by Table 1 and s-values given by A/V in eqn. (3).

There is a significant increase in the rate of precipitation with increasing surface area of the seed crystals and also with reduction in tube diameter, as expected.

Fig. 2 illustrates the total amount of precipitated gypsum and anhydrite present at any time t. Temperature and pressure have constant values of 50 °C and 1 atm, respectively.

Table 3. Seed specific surface area for various seed crystals.[14]

Seed	SSA/m^2 g^{-1}
A	0.66
B	1.25
C	1.31
D	0.28

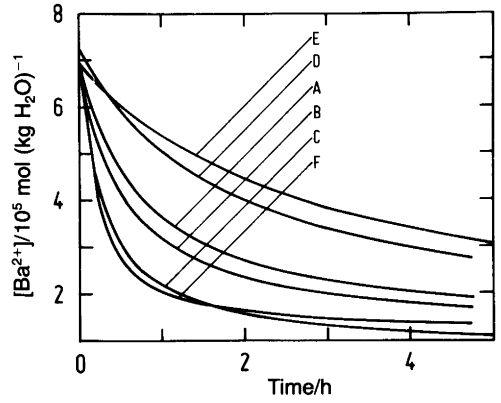

Fig. 1. Precipitation of $BaSO_4$ at T = 25 °C and P = 1 atm. Kinetic model. Curves A–D are obtained using eqn. (1) and experimental values of ks.[14] Curves E (tube segment diameter = 0.1 m) and F (tube segment diameter = 0.01 m) are obtained using eqn. (1) with k-values obtained from Table 1 and $s = A/V$.

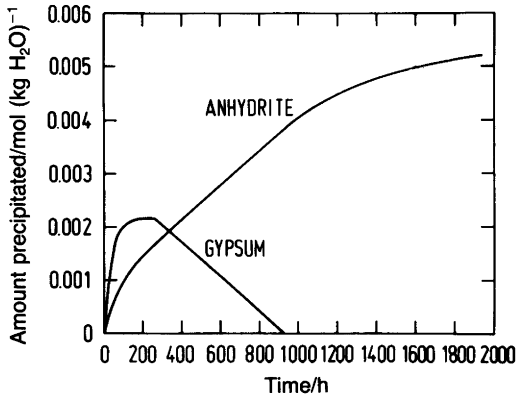

Fig. 2. Precipitation of $CaSO_4$ from a solution initially supersaturated in both gypsum and anhydrite. T = 50 °C. P = 1 atm. Kinetic model.

At this particular temperature and pressure anhydrite is the stable phase. Gypsum and anhydrite are treated independently in the calculation. Initially, therefore, both phases precipitate. After a certain time the solution becomes undersaturated in gypsum and this salt starts to dissolve. When gypsum has dissolved completely, anhydrite continues to precipitate at a relatively slow rate towards equilibrium.

Fig. 3 illustrates the amount of $BaSO_4$ precipitated at a composition of 10 % sea water and 90 % formation water as calculated by the equilibrium model.[2] The temperature is 91.4 °C and the pressure is 312 bar. At this water composition the amount of $BaSO_4$ is about 89.4 mg l^{-1}. The composition of the two waters which are mixed is given in Table 4.

The kinetic calculation also shown in Fig. 3 shows that after a certain period of time the amount of $BaSO_4$ precipitated is about 89.4 mg l^{-1}. This is the same amount as predicted by the equilibrium calculation.

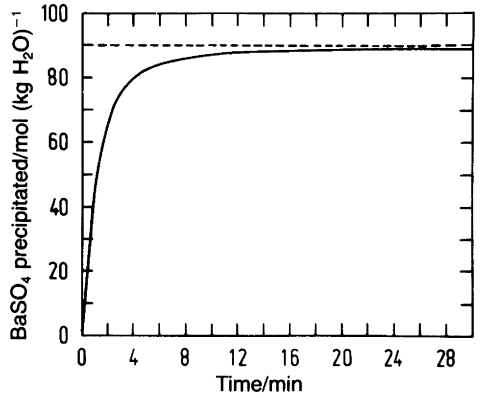

Fig. 3. Precipitation of $BaSO_4$ as a function of time for 10 % sea water and 90 % formation water. Water compositions are given in Table 4. T = 91.4 °C. P = 312 atm. (——) Kinetic model; (-----) equilibrium model.[2]

Table 4. Sea water and formation water compositions as given by chemical analysis at 1 atm and 20 °C.

Ion	Concentration/mg l^{-1}	
	Sea water	Formation water
Na^+	12465	14859
K^+	–	–
Mg^{2+}	1130	335
Ca^{2+}	450	1275
Sr^{2+}	9	335
Ba^{2+}	–	50
Cl^-	20950	26200
SO_4^{2-}	3077	–
HCO_3^-	170	415
pH	8.13	6.20

When the equilibrium, kinetic and flow models are combined, we may estimate mineral precipitation in a well area and in production tubing using eqn. (3) to determine s-values. In the well area, however, the specific area for crystal growth is much more uncertain. It may depend on many factors, including the geometry of the pore system. We have chosen an arbitrary number of 40 m^{-1} in order to demonstrate what kind of calculations we may perform using our model.

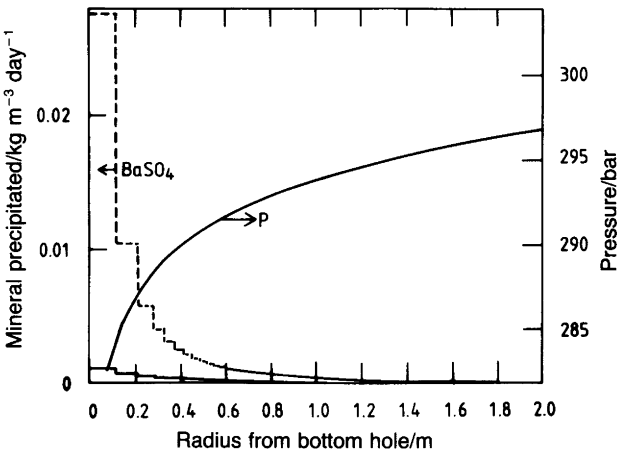

Fig. 4. Precipitation of $BaSO_4$ in the well area as a function of distance from the bottom hole. The waters were mixed 2 m from the centre of the tubing. (-----) Equilibrium model; (——) kinetic model. Oil flow rate = 1600 Sm^3 day^{-1}; watercut = 20 %; gas/oil ratio = 163.5 Sm^3/Sm^3; T = 70 °C; Sm^3 is at 15 °C and 1 atm.

As an example we have estimated the precipitation occurring if we produced a 90 % formation water – 10 % sea water mixture (data given in Table 4) from a well with a production rate of 1600 Sm^3 day^{-1} of oil with a watercut of 20 %, the gas–oil ratio being 163.5 Sm^3/Sm^3 at 15 °C and 1 atm total pressure.

From Fig. 4 it may be seen that $BaSO_4$ is precipitated in the well area in increasing amounts as the pressure is decreasing. The kinetic model gives lower values than the equilibrium model, as expected. The amount precipitated as given by Fig. 4 may be sufficient to reduce significantly the permeability of formation in the area near the well over a period of a few months. When the kinetic model is used to calculate this amount, however, the result is very dependent on the surface area for crystal growth.

The main precipitation of $CaCO_3$ occurs at the bubble-point pressure, 223.5 bar (at 1806 m from the top of the well), as can be observed from Fig. 5. This is in accordance with pH changes and shifts in the carbonate equilibria when CO_2(g) is leaving the solution.

In Fig. 6 the precipitation of $BaSO_4$ in the production tubing is shown. Mixing of the waters has taken place before the water enters the tubing. When the kinetic model is used to calculate the $BaSO_4$ precipitation, increasing precipitation is observed when the water flows up the tubing. This is due to increasing supersaturation as a result of delayed precipitation relative to an equilibrium situation. The equilibrium-based calculation shows a more-or-less constant precipitation slightly dependent on pressure and temperature changes. The abrupt changes occurring at 1806 and 450 m are due to effects of vaporization at the bubble point and the pressure change where the deviation angle of the well becomes vertical.

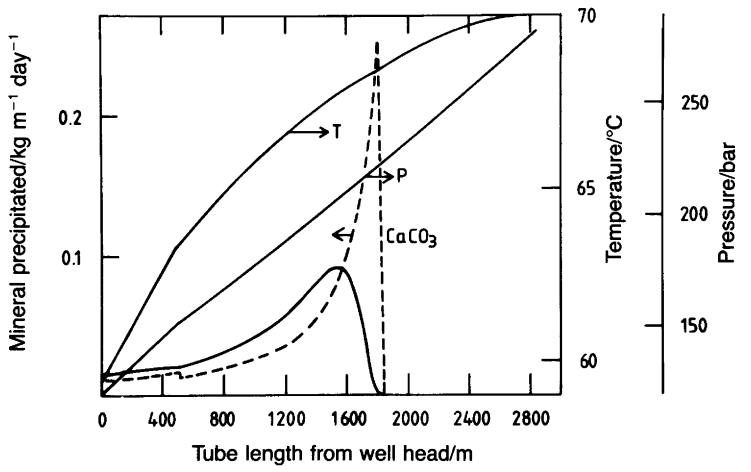

Fig. 5. Precipitation of $CaCO_3$ in the production tubing as a function of distance from the well head. (-----) Equilibrium model; (——) kinetic model. Oil flow rate = 1600 Sm^3 day^{-1}; watercut = 20 %; gas/oil ratio = 163.5 Sm^3/Sm^3; T_{well} = 70 °C; $T_{well\ head}$ = 59 °C; Sm^3 is at 15 °C and 1 atm.

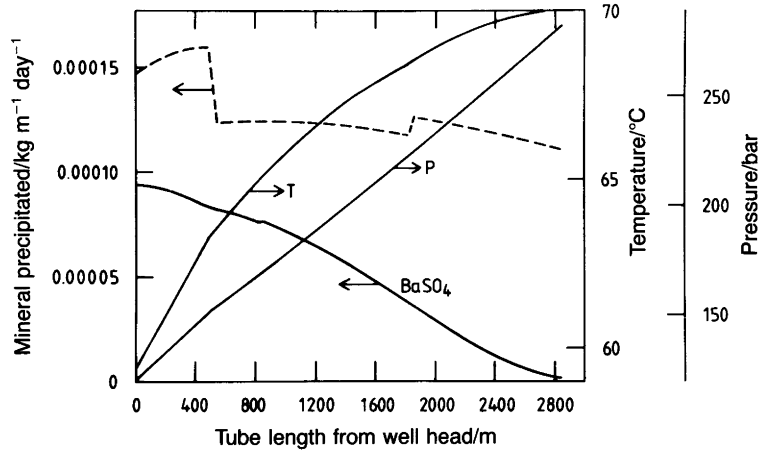

Fig. 6. Precipitation of $BaSO_4$ in the production tubing as a function of distance from the well head. (-----) Equilibrium model; (——) kinetic model. The mixing of injection and formation water has taken place in the well area. Oil flow rate = 1600 Sm^3 day^{-1}. watercut = 20 %; gas/oil ratio = 163.5 Sm^3/Sm^3; T_{well} = 70 °C; $T_{well\ head}$ = 59 °C; Sm^3 is at 15 °C and 1 atm.

In Fig. 7 the $BaSO_4$ precipitation is calculated on the assumption that 90 % formation water and 10 % sea water mix in the bottom of the tubing. As a consequence, a decreasing $BaSO_4$ precipitation is calculated as the mixed waters flow up the tubing. This situation is frequently observed in practice and results in thicker layers of scale close to the bottom of the well and smaller amounts at the top.

We have used our model to estimate the scale thickness profile in a production system where data are available to compare model and field data. Water compositions are given in Table 5. Ion tracking measurements over a period of 43 days after sea water breakthrough in this well showed that the Ba^{2+} content decreased, while the SO_4^{2-} content increased, thus indicating $BaSO_4$ scaling. An increase of sea water in the product water from 0 to 2 % over the same period was estimated. Inhibitors were not injected into this well, thus giving us an exellent opportunity to compare field observations with calculated data.

The well was shut for 43 days following sea-water breakthrough and the tubing pulled up for other reasons. The scale thickness in the tubing was then measured, and analysis showed that the scale consisted of > 90 % $BaSO_4$. The model curve shown in Fig. 8 was obtained by performing several simulations with a stepwise increase in the sea-water content from 0 to 2 % in four steps of 0.5 % over 10 + 10 + 10 + 13 days. The sea water and formation water values in Table 5 were used. The main assumption in the calculations was that sea water did not mix with formation water until these waters reached the bottom of the production tubing. In Fig. 8 the calculated results are compared with the measured scale thickness. A reasonable agreement is observed.

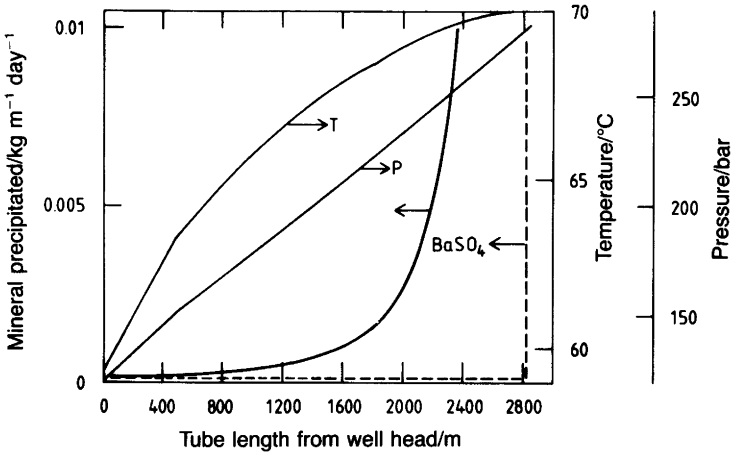

Fig. 7. Precipitation of $BaSO_4$ in the production tubing as a function of distance from the well head. (-----) Equilibrium model; (——) kinetic model. The mixing of injection and formation water has taken place in the bottom hole. Oil flow rate = 1600 Sm^3 day^{-1}; watercut = 20 %; Gas/oil ratio = 163.5 Sm^3/Sm^3; T_{well} = 70 °C; $T_{well\ head}$ = 59 °C; Sm^3 is at 15 °C and 1 atm. $BaSO_4$ precipitation at the point of mixing the water (2843 m): Equilibrium model, 1.48 kg m^{-1} day^{-1}. Kinetic model, 0.18 kg m^{-1} day^{-1}.

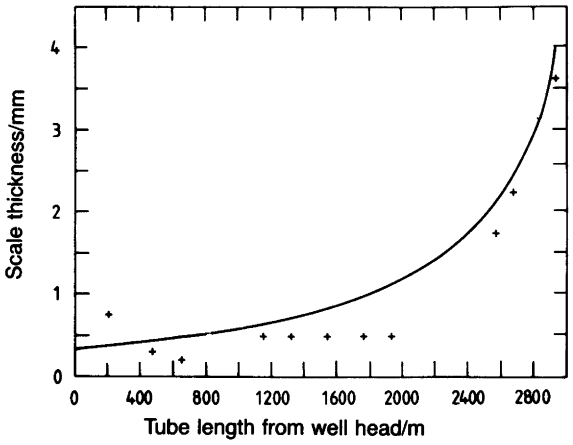

Fig. 8. Deposition of $BaSO_4$ in production tubing as a function of distance from the well head 43 days after sea water breakthrough. The mixing of formation water and sea water was done in four steps: 0.5 % sea water in 10 days, 1.0 % in 10 days, 1.5 % in 10 days and 2.0 % in 13 days. (——) Model: the mixing of injection water and formation water was performed in the bottom hole. Oil flow rate = 1792.2 Sm^3 day^{-1}; watercut = 57.5 %; gas/oil ratio = 196.0 Sm^3/Sm^3; well head pressure = 114 bar; bottom hole pressure = 312 bar; bottom hole temperature = 91.4 °C; well head temperature = 84 °C. (+) Measured.

We have investigated production data of many North Sea wells to obtain examples where similar comparisons between calculation and field data on mineral scaling could be performed. Lack of scaling data or inhibitor treatment, however, made all these wells unsuitable for such a comparison.

Table 5. Sea water and formation water compositions as given by chemical analysis at 1 atm and 20 °C.

Ion	Concentration/mg l^{-1}	
	Sea water	Formation water
Na^+	12100	9054
K^+	–	190
Mg^{2+}	1130	70
Ca^{2+}	450	300
Sr^{2+}	9	50
Ba^{2+}	–	60
Cl^-	20950	14300
SO_4^{2-}	2300	–
HCO_3^-	170	1100
pH	7.95	–

Conclusion

The present model is able to predict scale formation in oil production wells. Both the well area and the production tubing are considered. Important input data for the model calculations are representative water and gas analysis, together with production data.

The model predicts that the liquid movements along the pressure and temperature gradients results in delayed precipitation owing to variable rates of precipitation for the different minerals. The total precipitation is also less than that predicted by equilibrium calculations.

The present scaling model still rests on assumptions which may not be fulfilled during oil production. By improving our knowledge of mineral precipitation in flowing mixed oil–water system it should be possible to improve the present model.

Appendix 1. Rate equations after elimination and simplification

Eqns. (A1), (A2a)–(A6a), (A7) and (A8) are used for precipitation, while eqns. (A1), (A2b)–(A6b), (A7) and (A8) are used for dissolution.

$$\frac{d[CO_2(aq)]}{dt} = k_{-1}[H_2CO_3] - k_1[CO_2(aq)] + k_{-2}[HCO_3^-] - k_2[CO_2(aq)]\frac{K_w}{K_{A1}}\frac{[HCO_3^-]}{[H_2CO_3]} \quad \text{(A1)}$$

$$\frac{d[CaCO_3(s)]}{dt} = k_{prec,CaCO_3}\, s \left\{ \left[\{[Ca^{2+}]^\circ + [CaCO_3(s)]^\circ + [CaSO_4(s,A)]^\circ + [CaSO_4(s,G)]^\circ - [CaCO_3(s)] - [CaSO_4(s,A)] - [CaSO_4(s,G)]\} \times \left(\frac{K_{A2}}{K_{A1}}[HCO_3^-][HCO_3^-]/[H_2CO_3]\right) \right]^{1/2} - \left(\frac{K^\circ_{sp,CaCO_3}}{\gamma^2_{CaCO_3}}\right)^{1/2} \right\}^2 \quad \text{(A2a)}$$

$$\frac{d[CaSO_4(s,A)]}{dt} = k_{prec,CaSO_4(A)}\, s \left[\left(\{[Ca^{2+}]^\circ + [CaCO_3(s)]^\circ + [CaSO_4(s,A)]^\circ + [CaSO_4(s,G)]^\circ - [CaCO_3(s)] - [CaSO_4(s,A)] - [CaSO_4(s,G)]\} \times \{[CaSO_4(s,A)]^\circ + [BaSO_4(s)]^\circ + [SrSO_4(s)]^\circ + [SO_4^{2-}]^\circ + [CaSO_4(s,G)]^\circ - [CaSO_4(s,A)] - [BaSO_4(s)] - [SrSO_4(s)] - [CaSO_4(s,G)]\} \right)^{1/2} - \left(\frac{K^\circ_{sp,CaSO_4(A)}}{\gamma^2_{CaSO_4(A)}}\right)^{1/2} \right]^2 \quad \text{(A3a)}$$

$$\frac{d[BaSO_4(s)]}{dt} = k_{prec,BaSO_4}\, s \left[\left(\{[Ba^{2+}]^\circ + [BaSO_4(s)]^\circ - [BaSO_4(s)]\} \times \{[CaSO_4(s,A)]^\circ + [BaSO_4(s)]^\circ + [SrSO_4(s)]^\circ + [SO_4^{2-}]^\circ + [CaSO_4(s,G)]^\circ - [CaSO_4(s,A)] - [BaSO_4(s)] - [SrSO_4(s)] - [CaSO_4(s,G)]\} \right)^{1/2} - \left(\frac{K^\circ_{sp,BaSO_4}}{\gamma^2_{BaSO_4}}\right)^{1/2} \right]^2 \quad \text{(A4a)}$$

$$\frac{d[SrSO_4(s)]}{dt} = k_{prec,SrSO_4}\, s \left[\left(\{[Sr^{2+}]^\circ + [SrSO_4(s)]^\circ - [SrSO_4(s)]\} \times \{[CaSO_4(s,A)]^\circ + [BaSO_4(s)]^\circ + [SrSO_4(s)]^\circ + [SO_4^{2-}]^\circ + [CaSO_4(s,G)]^\circ - [CaSO_4(s,A)] - [BaSO_4(s)] - [SrSO_4(s)] - [CaSO_4(s,G)]\} \right)^{1/2} - \left(\frac{K^\circ_{sp,SrSO_4}}{\gamma^2_{SrSO_4}}\right)^{1/2} \right]^2 \quad \text{(A5a)}$$

$$\frac{d[CaSO_4(s,G)]}{dt} = k_{prec,CaSO_4(G)}\, s \left[\left(\{[Ca^{2+}]^\circ + [CaCO_3(s)]^\circ + [CaSO_4(s,A)]^\circ + [CaSO_4(s,G)]^\circ - [CaCO_3(s)] - [CaSO_4(s,A)] - [CaSO_4(s,G)]\} \times \{[CaSO_4(s,A)]^\circ + [BaSO_4(s)]^\circ + [SrSO_4(s)]^\circ + [SO_4^{2-}]^\circ + [CaSO_4(s,G)]^\circ - [CaSO_4(s,A)] - [BaSO_4(s)] - [SrSO_4(s)] - [CaSO_4(s,G)]\} \right)^{1/2} - \left(\frac{K^\circ_{sp,CaSO_4(G)}}{\gamma^2_{CaSO_4(G)}}\right)^{1/2} \right]^2 \quad \text{(A6a)}$$

$$\frac{d[CaCO_3(s)]}{dt} = -k_{diss,CaCO_3}\, s \left\{ \left[\left(\frac{K^\circ_{sp,CaCO_3}}{\gamma^2_{CaCO_3}}\right)^{1/2} - \{[Ca^{2+}]^\circ + [CaCO_3(s)]^\circ + [CaSO_4(s,A)]^\circ + [CaSO_4(s,G)]^\circ - [CaCO_3(s)] - [CaSO_4(s,A)] - [CaSO_4(s,G)]\} \times \left(\frac{K_{A2}}{K_{A1}}\frac{[HCO_3^-][HCO_3^-]}{[H_2CO_3]}\right) \right]^{1/2} \right\}^2 \quad \text{(A2b)}$$

$$\frac{d[CaSO_4(s,A)]}{dt} = -k_{diss,CaSO_4(A)}\, s \left[\left(\frac{K^\circ_{sp,CaSO_4(A)}}{\gamma^2_{CaSO_4(A)}}\right)^{1/2} - \left(\{[Ca^{2+}]^\circ + [CaCO_3(s)]^\circ + [CaSO_4(s,A)]^\circ + [CaSO_4(s,G)]^\circ - [CaCO_3(s)] - [CaSO_4(s,A)] - [CaSO_4(s,G)]\} \times \{[CaSO_4(s,A)]^\circ + [BaSO_4(s)]^\circ + [SrSO_4(s)]^\circ + [SO_4^{2-}]^\circ + [CaSO_4(s,G)]^\circ - [CaSO_4(s,A)] - [BaSO_4(s)] - [SrSO_4(s)] - [CaSO_4(s,G)]\} \right)^{1/2} \right]^2 \quad \text{(A3b)}$$

$$\frac{d[BaSO_4(s)]}{dt} = -k_{diss,BaSO_4}\, s \left[\left(\frac{K^\circ_{sp,BaSO_4}}{\gamma^2_{BaSO_4}}\right)^{1/2} - (\{[Ba^{2+}]^\circ + [BaSO_4(s)]^\circ - [BaSO_4(s)]\} \times \{[CaSO_4(s,A)]^\circ + [BaSO_4(s)]^\circ + [SrSO_4(s)]^\circ + [SO_4^{2-}]^\circ + [CaSO_4(s,G)]^\circ - [CaSO_4(s,A)] - [BaSO_4(s)] - [SrSO_4(s)] - [CaSO_4(s,G)]\})^{1/2} \right]^2 \quad \text{(A4b)}$$

$$\frac{d[SrSO_4(s)]}{dt} = -k_{diss,SrSO_4}\, s \left[\left(\frac{K^\circ_{sp,SrSO_4}}{\gamma^2_{SrSO_4}} \right)^{1/2} - (\{[Sr^{2+}]^\circ + [SrSO_4(s)]^\circ - [SrSO_4(s)]\} \times \{[CaSO_4(s,A)]^\circ + [BaSO_4(s)]^\circ + [SrSO_4(s)]^\circ + [SO_4^{2-}]^\circ + [CaSO_4(s,G)]^\circ - [CaSO_4(s,A)] - [BaSO_4(s)] - [SrSO_4(s)] - [CaSO_4(s,G)]\})^{1/2} \right]^2 \quad \text{(A5b)}$$

$$\frac{d[CaSO_4(s,G)]}{dt} = -k_{diss,CaSO_4(G)}\, s \left[\left(\frac{K^\circ_{sp,CaSO_4(G)}}{\gamma^2_{CaSO_4(G)}} \right)^{1/2} - (\{[Ca^{2+}]^\circ + [CaCO_3(s)]^\circ + [CaSO_4(s,A)]^\circ + [CaSO_4(s,G)]^\circ - [CaCO_3(s)] - [CaSO_4(s,A)] - [CaSO_4(s,G]\} \times \{[CaSO_4(s,A)]^\circ + [BaSO_4(s)]^\circ + [SrSO_4(s)]^\circ + [SO_4^{2-}]^\circ + [CaSO_4(s,G)]^\circ - [CaSO_4(s,A)] - [BaSO_4(s)] - [SrSO_4(s)] - [CaSO_4(s,G)]\})^{1/2} \right] \quad \text{(A6b)}$$

$$0 = \frac{[CO_2(aq)](\Sigma n_i^\circ - n_{CO_2})}{P^\circ_{tot} \times K_{H,CO_2(aq)} - [CO_2(aq)]} + K_{oil}[CO_2(aq)] + [CO_2(aq)] + [H_2CO_3] + \frac{K_{A2}}{K_{A1}} \frac{[HCO_3^-][HCO_3^-]}{[H_2CO_3]} + [HCO_3^-] + [CaCO_3(s)] - \{[CaCO_3(s)]^\circ + [CO_2(oil)]^\circ + [CO_2(aq)]^\circ + [H_2CO_3]^\circ + [HCO_3^-]^\circ + [CO_3^{2-}]^\circ + n^\circ_{CO_2}\} \quad \text{(A7)}$$

$$0 = 2([Ca^{2+}]^\circ + [CaCO_3(s)]^\circ + [Ba^{2+}]^\circ + [Sr^{2+}]^\circ - [SO_4^{2-}]^\circ - K(c) - 2[CaCO_3(s)] + \frac{K_{A1}[H_2CO_3]}{[HCO_3^-]} - [HCO_3^-] - 2\frac{K_{A2}}{K_{A1}} \frac{[HCO_3^-][HCO_3^-]}{[H_2CO_3]} - \frac{K_w}{K_{A1}} \frac{[HCO_3^-]}{[H_2CO_3]} - \frac{K_A([HA]^\circ + [A^-]^\circ)[HCO_3^-]}{K_A[HCO_3^-] + K_{A1}[H_2CO_3]} \quad \text{(A8)}$$

Appendix 2. List of symbols

$[CO_2(oil)]$/M	Concentration of CO_2(oil) at time t
P/atm	Pressure
$[CO_2(aq)]$/M	Concentration of CO_2(aq) at time t
$[H_2CO_3]$/M	Concentration of H_2CO_3 at time t
$[HCO_3^-]$/M	Concentration of HCO_3^- at time t
$[OH^-]$/M	Concentration of OH^- at time t
$[H^+]$/M	Concentration of H^+ at time t
$[CO_3^{2-}]$/M	Concentration of CO_3^{2-} at time t
$[A^-]$/M	Concentration of A^- at time t
[HA]/M	Concentration of HA at time t
$[CaCO_3(s)]$/M	Concentration of $CaCO_3$(s) at time t
$[Ca^{2+}]$/M	Concentration of Ca^{2+} at time t
$[CaSO_4(s,A)]$/M	Concentration of $CaSO_4$(s,A) at time t
$[SO_4^{2-}]$/M	Concentration of SO_4^{2-} at time t
$[BaSO_4(s)]$/M	Concentration of $BaSO_4$(s) at time t
$[Ba^{2+}]$/M	Concentration of Ba^{2+} at time t
$[SrSO_4(s)]$/M	Concentration of $SrSO_4$(s) at time t
$[Sr^{2+}]$/M	Concentration of Sr^{2+} at time t
$[CaSO_4(s,G)]$/M	Concentration of $CaSO_4$(s,G) at time t
n_i	Moles of i in gas at time t
$[i]^\circ$/M	Concentration of i at time $t = 0$
K°_{sp}	Thermodynamic solution product
K(c)/M	Σ Equivalent concentration of non-reacting ions
K_{A2}/M	$= [CO_3^{2-}][H^+]/[HCO_3^-]$
K_{A1}/M	$= [HCO_3^-][H^+]/[H_2CO_3]$
K_A/M	$= [A^-][H^+]/[HA]$
K_w/M^2	$= [H^+][OH^-]$
$K_{H,CO_2(aq)}$/M atm^{-1}	$= [CO_2(aq)]/P_{CO_2}$
K_{oil}	$= [CO_2(oil)]/[CO_2(aq)]$
γ	Mean activity coefficient
s/m^{-1}	Specific surface area
k	Rate constant

References

1. Haarberg, T., Seim, I., Skjørholm, S. J., Østvold, T., Read, P. and Schmidt, T. Third International Symposium on Chemicals in the Oil Industry, Manchester, April 19–20, 1988. *Unpublished.*

2a. Haarberg, T., Granbakken, D. B., Rollheim, M., Østvold, T., Read, P. and Schmidt, T. *SPE Production Engineering. In press.*

2b. Haarberg, T., Jacobsen, J. E. and Østvold, T. *Acta Chem. Scand., Ser. A 44* (1990) 907.

3. Nancollas, G. H., Sawada, K. and Schuttringer, E. In: Westbroek, P. and deJong, E. W., Eds., *Biomineralization and Biological Metal Accumulation,* Reidel, Dordrecht 1983, pp. 155–169.

4. Nancollas, G. H. and Reddy, M. M. *Soc. Pet. Eng. J.* (April 1974) 117.

5. Reddy, M. M. and Nancollas, G. H. *Desalination 12* (1973) 61.

6. Kazmierczak, T. F., Tomson, M. B. and Nancollas, G. H. *J. Phys. Chem. 86* (1982) 103.

7. Gardner, G. L. and Nancollas, G. H. *J. Phys. Chem. 87* (1983) 4699.
8. Liu, S. T., Nancollas, G. H. and Gasiecki, E. A. *J. Cryst. Growth 33* (1976) 11.
9. Leung, W. H. and Nancollas, G. H. *J. Cryst. Growth 44* (1978) 163.
10. Leung, W. H. and Nancollas, G. H. *J. Inorg. Nucl. Chem. 40* (1978) 1871.
11. Rizkalla, E. N. *J. Chem. Soc., Faraday Trans. 1, 79* (1983) 1857.
12. Söhnel, O. and Handlirová, M. *Industrial Crystallization 1984,* Elsevier, Amsterdam 1984, p. 281.
13. Liu, S. T. and Nancollas, G. H. *J. Colloid Interface Sci. 52* (1975) 582.
14. Nancollas, G. H. and Liu, S. T. *Soc. Pet. Eng. J.* (Dec. 1975) 509.
15. Söhnel, O. and Handlirová, M. *Cryst. Res. Technol. 19* (1984) 477.
16. Campbell, J. R. and Nancollas, G. H. *J. Phys. Chem. 73* (1969) 1735.
17. Nancollas, G. H., Eralp, A. E. and Gill, J. S. *Soc. Pet. Eng. J.* (April 1978) 133.
18. Nancollas, G. H. and Gill, J. S. *Soc. Pet. Eng. J.* (Dec. 1979) 423.
19. Austin, A. E., Miller, J. F., Richard, N. A. and Kircher, J. F. *Desalination 16* (1975) 331.
20. Liu, S. T. and Nancollas, G. H. *J. Colloid Interface Sci. 52* (1975) 593.
21. Gill, J. S. and Nancollas, G. H. *J. Cryst. Growth 48* (1980) 34.
22. Liu, S. T. and Nancollas, G. H. *J. Cryst. Growth 6* (1970) 281.
23. Nancollas, G. H., Reddy, M. M. and Tsai, F. *J. Cryst. Growth 20* (1973) 125.
24. Liu, S. T. and Nancollas, G. H. *J. Inorg. Nucl. Chem. 33* (1971) 2311.
25. Sjøberg, E. L. *Thesis,* Institute of Geology, University of Stockholm, Stockholm, Sweden 1978.
26. Østvold, T. and Rollheim, M. Symposium on Oil Field Chemicals, Geilo, March 11–13, 1991. *Unpublished.*
27. Nancollas, G. H., White, W., Tsai, F. and Maslow, L. *CORROSION-NACE 35,* No. 7 (1979) 304.
28. Cheng, V. K., Coller, B. A. W. and Powell, J. L. *Faraday Discuss. Chem. Soc. 77* (1984) 243.
29. Welch, M. J., Lifton, J. F. and Seck, J. A. *J. Phys. Chem. 73* (1969) 3351.
30. Pinsent, B. R. W., Pearson, L. and Roughton, F. J. W. *Trans. Faraday Soc. 52* (1956) 1512.
31. Dake, L. P. *Fundamentals of Reservoir Engineering,* Elsevier, Amsterdam 1978, p. 131.
32. Exploration Consultants Ltd. *VFP Reference Manual Exploration Consultants Ltd.,* Oxfordshire, UK 1987.

Received February 20, 1991.